AAS 14-263

NAVIGATION DESIGN AND ANALYSIS FOR THE ORION EARTH-MOON MISSION

Christopher D'Souza*, and Renato Zanetti†

This paper details the design of the cislunar optical navigation system being proposed for the Orion Earth-Moon (EM) missions. In particular, it presents the mathematics of the navigation filter. The unmodeled accelerations and their characterization are detailed. It also presents the analysis that has been performed to understand the performance of the proposed system, with particular attention paid to entry flight path angle constraints and the ΔV performance.

INTRODUCTION

Vehicles navigating to or from the Moon usually rely on ground tracking and ground updates to perform the insertion and correction maneuvers. A natural advancement in technology is autonomy. The Orion vehicle, designed to explore space beyond LEO, is required to return the crew safely in the case of loss of communication with the ground. As such, it needs to be able to navigate autonomously, independent of ground-based measurements, utilizing on-board sensors subject to stringent mass/power/volume constraints. Since the vehicle will be carrying optical cameras, the cislunar navigation system is designed to use images obtained from these cameras, in particular star/planetary limb and planetary disk measurements. Whereas the navigation system of Orion in and below LEO is well understood, the design of the cislunar navigation system unique presents challenges.

Whereas the Orion sensor complement includes two star trackers, the star trackers being considered have a very limited field-of-view. As such, they don't lend themselves to cislunar optical navigation, which needs fields-of-view in excess of 20 degrees. Thus, optical cameras, which are already planned for situational awareness, are harnessed into a cislunar navigation role. In this paper the design of the cislunar optical navigation system being proposed for the Orion Earth-Moon (EM) missions is presented. In particular, it will present the mathematics of the navigation filter and the analysis that has been performed to understand the performance of the proposed system, with particular attention paid to entry flight path angle constraints and the DV performance.

Previus studies focused on the lunar orbit determination problem [1, 2]. Tuckness and Young consider autonomous navigation for lunar transfers [3]. Their analysis focuses on azimuth and elevation measurements of the Earth, Moon, and Sun. Two star-elevation measurements relative to the planet's limb provide the same kind of information as azimuth and elevation of the apparent center of the planet. However, star-elevation measurements are the preferred approach for two reasons. First,

*GN&C Autonomous Flight Systems Engineer, Aeroscience and Flight Mechanics Division, NASA Johnson Space Center EG6, 2101 NASA Parkway, Houston, Texas, 77058. chris.dsouza@nasa.gov

†GN&C Autonomous Flight Systems Engineer, Aeroscience and Flight Mechanics Division, NASA Johnson Space Center EG6, 2101 NASA Parkway, Houston, Texas, 77058. renato.zanetti@nasa.gov

multiple stars can be processed simultaneously, and the redundant information effectively filters out some noise. Second, the method used here does not depend on the attitude of the spacecraft, or on the misalignments of the sensors, reducing the possible error sources. Christian and Lightsey [5] provide an overview of many possible options to autonomously navigate in Cislunar space.

This work builds on previous results presented in [4] but focuses on new analysis done to characterize the process noise, i.e. unmodeled accelerations, and the preliminary results of the EM1 navigation system design. This investigation specifically addresses the transfer from the Moon to the Earth. In an emergency situation, during a loss of communication scenario, the primary objective is the safety of the crew. This subsequently translates into a flight-path angle requirement at entry interface (EI) for a direct entry. A direct entry, as opposed to a skip entry, reduces the risk of the capsule bouncing back into space, and allows for a greater margin on the flight-path angle at EI.

The accuracy of the flight-path angle at EI is driven by several factors including the navigation, targeting, and burn execution errors at the time of the last mid-course maneuver, and unaccounted trajectory perturbations between the last mid-course maneuver and EI. Apollo missions tolerated a maximum flight path angle error at EI of ± 1 degree, with half of this error allocated to navigation. A similar criterion is employed in this study.

Perturbations are a major source of errors in the cislunar navigation performance of Orion. In a perfect world all the sources of perturbations would be modeled in the filter dynamics. However, computational limitations preclude such extensive modeling. Therefore, the primary sources of perturbations are characterized. In particular there are three categories of unmodeled acceleration: propulsive sources, gravitational perturbations, and solar radiation pressure. Only propulsive errors are included in this analysis; the gravitational and solar radiation pressure are not included – they will be included in a future study. For EM1, the gravitational and solar radiation pressure errors are several orders of magnitude below the thrusting sources. The propulsive sources considered are: attitude deadbands, attitude slews, CO2 venting, and sublimator venting.

Linear covariance techniques are used to perform the analysis for the Orion Cislunar missions. This comports well for the navigation system design since the cislunar navigation system on Orion will be an Extended Kalman Filter. Many of the same states and dynamics used in the linear covariance analysis will be used in the on-board cislunar navigation system. A preliminary design of the cislunar navigation system is presented. This is supported by linear covariance analyses which provides navigation performance, trajectory dispersion performance and ΔV usage.

The paper is organized as follows: Section 2 will contain a brief description of linear covariance analysis. In Section 3, the navigation system will be described. Section 4 will contain a description of the perturbations used in this analysis. Section 5 will contain results of this analysis. Finally, some concluding comments will be made in Section 6.

LINEAR COVARIANCE ANALYSIS

This investigation is performed using linear covariance (LinCov) analysis techniques [6, 7]. The state vector is given by [4]

$$\mathbf{x} = \begin{Bmatrix} \mathbf{r}^{\mathrm{T}} & \mathbf{v}^{\mathrm{T}} & \boldsymbol{\theta}^{\mathrm{T}} & \mathbf{b}_m^{\mathrm{T}} & \boldsymbol{\sigma}_m^{\mathrm{T}} & \boldsymbol{\gamma}_m^{\mathrm{T}} & \mathbf{b}_r^{\mathrm{T}} & b_{st} & b_{ss,earth} & b_{ss,moon} & b_{h,earth} & b_{h,moon} \end{Bmatrix}^{\mathrm{T}}. \tag{1}$$

The nominal trajectory is obtained by integrating the nominal dynamics model with an Encke-Nystrom method [8]. Neither the rotation vector $\boldsymbol{\theta}$ nor its uncertainty are integrated in this analysis.

The nominal attitude is known at any time and it does not need to be calculated. The attitude estimation error covariance is constant and is driven by the star tracker accuracy. The attitude navigation dispersion covariance is constant and is given by the attitude control dead-band. The attitude environment dispersion covariance is constant and obtained from the above two quantities assumed uncorrelated. Before the star elevation is determined, the vehicle slews in preparation for measurement acquisition. This attitude maneuver is performed by the onboard thrusters and is assumed to be instantaneous. Due to thruster misalignment, this maneuver adds uncertainty to the translational states. After the batch of measurements is available, the vehicle returns to its nominal attitude. In linear covariance analysis, the difference between the true state and the nominal state is defined as the environment dispersion

$$\delta\mathbf{x} \triangleq \mathbf{x} - \bar{\mathbf{x}}. \tag{2}$$

The difference between the estimated state and the nominal state is defined as the navigation dispersion

$$\delta\hat{\mathbf{x}} \triangleq \hat{\mathbf{x}} - \bar{\mathbf{x}}. \tag{3}$$

Finally, the difference between the true state and the estimated state, is defined as the estimation error, sometimes referred to as the onboard navigation error

$$\mathbf{e} \triangleq \mathbf{x} - \hat{\mathbf{x}}. \tag{4}$$

Following the standard Kalman filter assumptions, the difference between the nominal and estimated models is represented with zero-mean, white noise. The estimated state evolves as

$$\dot{\hat{\mathbf{x}}} = \mathbf{f}(\hat{\mathbf{x}}), \tag{5}$$

where $\mathbf{f}$ is a nonlinear function representing the system dynamics as modeled by the filter. The evolution of the nominal state is modeled as

$$\dot{\bar{\mathbf{x}}} = \bar{\mathbf{f}}(\bar{\mathbf{x}}) = \mathbf{f}(\bar{\mathbf{x}}) + \boldsymbol{\upsilon}, \tag{6}$$

where $\bar{\mathbf{f}}$ is a nonlinear function representing the state dynamics as modeled in designing the nominal trajectory. The nominal dynamics $\bar{\mathbf{f}}$ may be higher fidelity than the filter's dynamics $\mathbf{f}$. The vector $\boldsymbol{\upsilon}$ represents the dynamics modeled in the nominal trajectory but neglected in the filter models. In Kalman filtering, the difference between the true dynamics and the filter's dynamics is called process noise. While these unmodeled dynamics are not actually white noise, they are modeled as such. The power spectral density of process noise is then tuned to achieve good performance. The same procedure is used here. In order to capture the difference between the two dynamical models, $\boldsymbol{\upsilon}$ is modeled as a zero-mean white process with spectral density $\hat{\mathbf{Q}}$. The goal is to represent the increased value of the navigation dispersion during propagation due to the difference between the nominal and filter's dynamical models.

The evolution of the navigation dispersion can be approximated to first-order as

$$\dot{\delta\hat{\mathbf{x}}} = \dot{\hat{\mathbf{x}}} - \dot{\bar{\mathbf{x}}} = \mathbf{f}(\bar{\mathbf{x}} + \delta\hat{\mathbf{x}}) - \mathbf{f}(\bar{\mathbf{x}}) - \boldsymbol{\upsilon} \simeq \mathbf{F}(\bar{\mathbf{x}})\delta\hat{\mathbf{x}} - \boldsymbol{\upsilon}. \tag{7}$$

The evolution of the navigation dispersion covariance is governed by

$$\dot{\hat{\mathbf{P}}} = \mathbf{F}(\bar{\mathbf{x}})\hat{\mathbf{P}} + \hat{\mathbf{P}}\mathbf{F}(\bar{\mathbf{x}})^{\mathrm{T}} + \hat{\mathbf{Q}}. \tag{8}$$

Similarly, the true state is modeled to evolve as

$$\dot{\mathbf{x}} = \mathbf{f}(\mathbf{x}) + \boldsymbol{\nu}. \tag{9}$$

The evolution of the estimation error is given by

$$\dot{\mathbf{e}} = \dot{\mathbf{x}} - \dot{\hat{\mathbf{x}}} \simeq \mathbf{f}(\bar{\mathbf{x}}) + \mathbf{F}(\bar{\mathbf{x}})(\mathbf{x} - \bar{\mathbf{x}}) + \boldsymbol{\nu} - \mathbf{f}(\bar{\mathbf{x}}) - \mathbf{F}(\bar{\mathbf{x}})(\hat{\mathbf{x}} - \bar{\mathbf{x}}) = \mathbf{F}(\bar{\mathbf{x}})\mathbf{e} + \boldsymbol{\nu}. \tag{10}$$

Vector $\boldsymbol{\nu}$ is modeled as zero mean white noise with spectral density $\mathbf{Q}$. The onboard covariance $\mathbf{P}$ evolves as

$$\dot{\mathbf{P}} = \mathbf{F}(\bar{\mathbf{x}})\mathbf{P} + \mathbf{P}\mathbf{F}(\bar{\mathbf{x}}) + \mathbf{Q}. \tag{11}$$

Notice that the Jacobian $\mathbf{F}$ could be evaluated at the estimated state $\hat{\mathbf{x}}$ instead of the nominal state $\bar{\mathbf{x}}$, as in the extended Kalman filter.

Finally

$$\delta\dot{\mathbf{x}} = \dot{\mathbf{x}} - \dot{\bar{\mathbf{x}}} \simeq \mathbf{F}(\bar{\mathbf{x}})\delta\mathbf{x} + \boldsymbol{\nu} - \boldsymbol{\upsilon} \tag{12}$$

and $\bar{\mathbf{P}}$ evolves as

$$\dot{\bar{\mathbf{P}}} = \mathbf{F}(\bar{\mathbf{x}})\bar{\mathbf{P}} + \bar{\mathbf{P}}\mathbf{F}(\bar{\mathbf{x}}) + \bar{\mathbf{Q}}. \tag{13}$$

Notice that $\bar{\mathbf{Q}} = \mathbf{Q} + \hat{\mathbf{Q}}$ if $\boldsymbol{\nu}$ and $\boldsymbol{\upsilon}$ are assumed to be uncorrelated.

Since the environment and navigation dispersions are naturally correlated, it is intuitive to create an augmented dispersion state, whose covariance is defined as $\boldsymbol{\Pi}$

$$\boldsymbol{\Pi} \triangleq \mathrm{E}\left\{ \begin{bmatrix} \delta\mathbf{x} \\ \delta\hat{\mathbf{x}} \end{bmatrix} \begin{bmatrix} \delta\mathbf{x} \\ \delta\hat{\mathbf{x}} \end{bmatrix}^{\mathrm{T}} \right\} = \begin{bmatrix} \bar{\mathbf{P}} & \mathbf{C} \\ \mathbf{C}^{\mathrm{T}} & \hat{\mathbf{P}} \end{bmatrix}, \tag{14}$$

$$\mathbf{C} \triangleq \mathrm{E}\left\{ \delta\mathbf{x}\, \delta\hat{\mathbf{x}}^{\mathrm{T}} \right\}. \tag{15}$$

The evolution of the augmented covariance is given by

$$\dot{\boldsymbol{\Pi}} = \begin{bmatrix} \mathbf{F}(\bar{\mathbf{x}}) & \mathbf{O}_{3\times3} \\ \mathbf{O}_{3\times3} & \mathbf{F}(\bar{\mathbf{x}}) \end{bmatrix} \boldsymbol{\Pi} + \boldsymbol{\Pi} \begin{bmatrix} \mathbf{F}(\bar{\mathbf{x}}) & \mathbf{O}_{3\times3} \\ \mathbf{O}_{3\times3} & \mathbf{F}(\bar{\mathbf{x}}) \end{bmatrix}^{\mathrm{T}} + \begin{bmatrix} \bar{\mathbf{Q}} & \hat{\mathbf{Q}} \\ \hat{\mathbf{Q}} & \hat{\mathbf{Q}} \end{bmatrix}, \tag{16}$$

where it is assumed that $\boldsymbol{\nu}$ and $\boldsymbol{\upsilon}$ are uncorrelated. All error states are modeled as first order Markov processes and are assumed to be uncorrelated to each other.

THE ORION CISLUNAR NAVIGATION FILTER

The Filter Dynamics

Since this filter operates once Orion is away from Earth (and outside of GPS range), the primary forces governing the motion of the vehicle are the gravitational forces of the Earth, the Moon, and the Sun. The trajectory is designed taking into account all three of these bodies. Whereas the equations of motion are formulated with respect to a central body, this (central body) changes depending on which sphere of influence the vehicle is subject to.

The equations of motion for the Earth-Sun-Moon system are

$$\ddot{\mathbf{r}}_{PV} = -\frac{\mu_P}{r_{PV}^3}\mathbf{r}_{PV} - \mu_Q \left[\frac{\mathbf{r}_{QV}}{r_{QV}^3} + \frac{\mathbf{r}_{PQ}}{r_{PQ}^3} \right] - \mu_S \left[\frac{\mathbf{r}_{SV}}{r_{SV}^3} + \frac{\mathbf{r}_{PS}}{r_{PS}^3} \right] \tag{17}$$

where and $\mathbf{r}_{PV}$ is the position of the vehicle (V) with respect to the primary body (P), $\mathbf{r}_{QV}$ is the position of the vehicle with respect to the secondary body (Q), $\mathbf{r}_{PQ}$ is the position of the secondary body with respect to the primary body, $\mathbf{r}_{SV}$ is the position of the vehicle with respect to the Sun (S), and $\mathbf{r}_{PS}$ is the position of the Sun with respect to the primary body. The geometry is shown in Figure 2. In many applications, these equations are integrated by a Runge-Kutta or Runge-Kutta-Fehlberg fixed-step or variable-step algorithms.

However, blindly applying a standard fourth-order Runge-Kutta method can lead to numerical errors (if large step sizes are taken) not to mention inefficiencies (if small step sizes are taken). The Encke-Nyström method has been shown to have none of these deficiencies – large step sizes can be taken and numerical precision maintained at the same time.

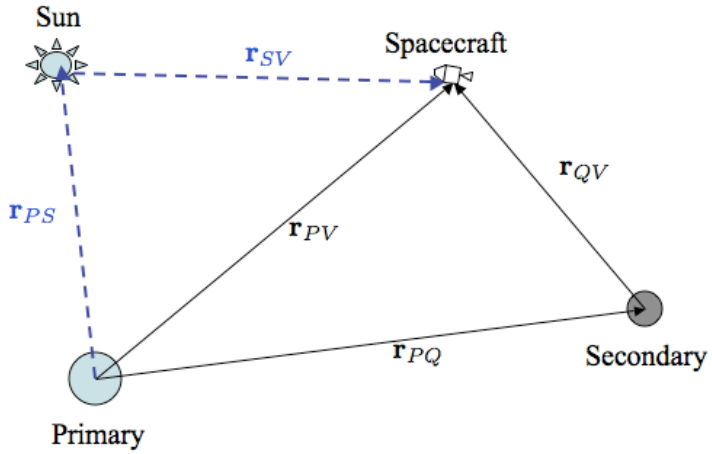

Figure 1. The Earth-Sun-Moon-Vehicle Geometry

The Encke-Nyström Method The Encke-Nyström method has an illustrious legacy. Unlike the Cowell's method, only the perturbations away from two-body motion are integrated. As such, the perturbations being integrated are small and excellent numerical precision is retained. In addition, since the force-field under which the equations of motion being integrated is conservative, and since the velocity derivatives are expressed in terms of the position only, a Nyström formulation of integration is used. The disadvantage of this method is that there is a bit of mathematical set-up required. However, if one is willing to pay this price, the dividends are enormous – both in terms of precision and computation time. The equations which are integrated are as follows:

$$\ddot{\mathbf{r}}_{PV} = -\frac{\mu_P}{r_{PV}^3}\mathbf{r}_{PV} - \frac{\mu_Q}{r_{QV}^3}\left[f(q_Q)\mathbf{r}_{PQ} + \mathbf{r}_{PV}\right] - \frac{\mu_S}{r_{SV}^3}\left[f(q_S)\mathbf{r}_{PS} + \mathbf{r}_{PV}\right] \tag{18}$$

where

$$\begin{aligned} q_{()} &= \frac{\left(\mathbf{r}_{PV} - 2\mathbf{r}_{P()}\right) \cdot \mathbf{r}_{PV}}{r_{P()}^2} \\ f(q_{()}) &= q_{()} \frac{3 + 3q_{()} + q_{()}^2}{1 + \left(1 + q_{()}\right)^{3/2}} \end{aligned}$$

This formulation was used in the Apollo program [8]. It should be noted that Eqs.(17) and (18) are mathematically equivalent.

The Trajectory Partials In order to compute the state transition matrix from an epoch to another epoch in the future (or the past), the partial of the future (or past) state with respect to the initial epoch must be computed. The reason the Encke-Nyström algorithm is introduced into this discussion is that the Encke-Nyström method is predicated on "small" deviations from a reference (osculating) orbit. This is precisely the foundation upon which the state transition matrix for the cislunar trajectory is built and it is also the foundation upon which linear covariance analysis is built. Whereas the state transition matrix is defined as

$$\begin{aligned} \Phi(t, t_0) &= \left(\frac{\partial \mathbf{X}(t)}{\partial \mathbf{X}(t_0)} \right)_{\mathbf{X}_{nom}} \\ &= \left[\begin{array}{cc} \frac{\partial \mathbf{r}}{\partial \mathbf{r}_0} & \frac{\partial \mathbf{r}}{\partial \mathbf{v}_0} \\ \frac{\partial \mathbf{v}}{\partial \mathbf{r}_0} & \frac{\partial \mathbf{v}}{\partial \mathbf{v}_0} \end{array} \right]_{\mathbf{X}_{nom}} \end{aligned}$$

the partials of the dynamics are defined as

$$\mathbf{A}(t) = \left(\frac{\partial \dot{\mathbf{X}}}{\partial \mathbf{X}} \right)_{\mathbf{X}_{nom}} (t).$$

With the dynamics defined in Eq. (40), the partials of the dynamics are found to be

$$\mathbf{A}(t) = \left[\begin{array}{cc} \mathbf{0}_{3\times3} & \mathbf{I}_3 \\ \mathbf{G}(t) & \mathbf{0}_{3\times3} \end{array} \right] \tag{19}$$

where $\mathbf{G}(t)$ is defined as

$$\begin{aligned} \mathbf{G}(t) &= -\frac{\mu_P}{r_{PV}^3} \left(I_3 - 3\frac{\mathbf{r}_{PV}\mathbf{r}_{PV}^T}{r_{PV}^2} \right) - \frac{\mu_Q}{r_{QV}^3} I_3 - \frac{\mu_S}{r_{SV}^3} I_3 + 3\mu_Q \left(f(q_Q)\mathbf{r}_{PQ} + \mathbf{r}_{PV} \right) \frac{\mathbf{r}_{QV}^T}{r_{QV}^5} \\ &\quad + 3\mu_S \left(f(q_S)\mathbf{r}_{PS} + \mathbf{r}_{PV} \right) \frac{\mathbf{r}_{SV}^T}{r_{SV}^5} - \mu_Q \frac{\mathbf{r}_{PQ}}{r_{QV}^3} \frac{\partial f(q_Q)}{\partial \mathbf{r}_{PV}} - \mu_S \frac{\mathbf{r}_{PS}}{r_{SV}^3} \frac{\partial f(q_S)}{\partial \mathbf{r}_{PV}} \end{aligned}$$

In the preceding equation, $\frac{\partial f(q_{()})}{\partial \mathbf{r}_{PV}}$ is defined as

$$\frac{\partial f(q_{()})}{\partial \mathbf{r}_{PV}} = f_{q_{()}}(q_{()}) \frac{2\left(\mathbf{r}_{PV} - \mathbf{r}_{P()}\right)^T}{r_{P()}^2}$$

and

$$f_{q_{()}}(q_{()}) = \frac{[3 + 3q_{()}(2 + q_{()})](1 + (1 + q_{()})^{3/2}) - 1.5q_{()}(3 + 3q_{()} + q_{()}^2)\sqrt{q_{()} + 1}}{(1 + (1 + q_{()})^{3/2})^2}.$$

The Measurements

Optical measurements are processed every 60 seconds. The optical camera has a 18 degree Field of View. The optical measurements consist of star-horizon measurements and apparent angular radius measurements. These measurements take into account when the planet is both larger than and smaller than the field of view. For a comprehensive description of the measurement models utilized in the filter see section IV of reference [4].

UNMODELED ACCELERATION CHARACTERIZATIONS

There are three categories of unmodeled acceleration with which a vehicle in cislunar space has to contend: propulsive sources, gravitational perturbations, and solar radiation pressure. Only propulsive errors are included in this analysis; the gravitational and solar radiation pressure are not included – they are several orders of magnitude below the propulsive sources. The propulsive sources, therefore, can be further separated into thruster errors and ECLSS (Environmental Control and Life Support System). Thruster errors include attitude deadbanding and attitude slewing maneuvers. ECLSS sources include Pressure Swing Adsorption (PSA) (CO_2 venting), ammonia sublimator venting, and waste water venting events. EM1 will have a 'metabolic simulator' which will exercise the entire ECLSS system except for waste water vents; hence waste water venting perturbations are not included in this analysis.

Attitude Dead-banding Maneuver Errors

Given a 24-jet ESA-SM config, with attitude dead-bands with 0.028 second on-time, the expected ΔV is

$$\Delta V = \begin{bmatrix} -8.2E-4 \\ 8.2E-4 \\ 1.0E-20 \end{bmatrix} \text{ ft/sec} \tag{20}$$

and assume that there is one firing every 30 minutes*. This means that there is a 1σ ΔV (assuming no inertial direction preference) of

$$\sigma_{\Delta V,RSS} = 1.160 \times 10^{-3} \text{ ft/sec} \iff \sigma_{\Delta V,Peraxis} = 6.695 \times 10^{-4} \text{ ft/sec} \tag{21}$$

This gives a process noise of

$$Q_{Att\ Deadband} = \frac{\sigma^2_{\Delta V,Peraxis}}{1800\,\text{sec}} = 2.490 \times 10^{-10} \text{ ft}^2/\text{sec}^3 \tag{22}$$

Attitude Slew Maneuver Errors

For attitude maneuvers, assume 25 attitude events, resulting in 50 slews over the mission, given a mission time of 160 hours. This can be thought of (and spread out) as one attitude slew every 3.2 hours. These events are as follows: 7 maneuvers (14 slews), 7 optical passes (14 slews), 10 communication passes (20 slews), 1 other attitude event (2 slews).

*Rodolfo Gonzales, 4/12/2013

Given a slew maneuver with a 0.7 second on-time with a 24 jet configuration, the residual error in body coordinates is

$$\Delta V = \begin{bmatrix} -2.4E-2 \\ 2.4E-2 \\ 1.0E-4 \end{bmatrix} \text{ ft/sec} \tag{23}$$

The 1 sigma error is

$$\sigma_{\Delta V,RSS,Slews} = 3.394 \times 10^{-2} \text{ ft/sec} \iff \sigma_{\Delta V,Peraxis,Slews} = 1.960 \times 10^{-2} \text{ ft/sec} \tag{24}$$

So, the process noise for attitude events with a 24-jet configuration is

$$Q_{AttSlews} = \frac{\sigma^2_{\Delta V,Peraxis,Slews}}{11520\,\text{sec}} = 3.335 \times 10^{-8} \text{ ft}^2/\text{sec}^3 \tag{25}$$

For the case of continuous tracking, with a pan/tilt camera, there will be less need for attitude slews to perform celestial navigation. Hence it is assumed that there will be 7 fewer attitude events, for a total of 18 attitude events, resulting in 36 slews over the mission, given the same mission time as before, resulting in one slew every 4.44 hours. The process noise is

$$Q_{AttSlews} = \frac{\sigma^2_{\Delta V,Peraxis,Slews}}{16000\,\text{sec}} = 2.401 \times 10^{-8} \text{ ft}^2/\text{sec}^3 \tag{26}$$

For the case of 12 attitude events (24 slews), this will result in one attitude slew ever 6.66 hours. So, the process noise for attitude events with a 24-jet configuration is

$$Q_{AttSlews} = \frac{\sigma^2_{\Delta V,Peraxis,Slews}}{24000\,\text{sec}} = 1.601 \times 10^{-8} \text{ ft}^2/\text{sec}^3 \tag{27}$$

Finally for the limiting case of only 6 attitude events (12 slews), we will have one attitude slew every 13.33 hours, resulting in a process noise of

$$Q_{AttSlews} = \frac{\sigma^2_{\Delta V,Peraxis,Slews}}{48000\,\text{sec}} = 8.003 \times 10^{-9} \text{ ft}^2/\text{sec}^3 \tag{28}$$

PSA Puffs

The Pressure Swing Adsorption (PSA) cycles automatically every 6-10 minutes, less during crew sleep periods, more when the crew is awake. The PSA system can be commanded to force a complete desaturation (all vents open into space) and then they would likely not open automatically for 40-60 minutes[†]. This would be needed during ground tracking passes and optical navigation passes.

The ΔV resulting from the PSA puffs can be calculated as follows: the force during a single vent is 36 lb-force and it lasts for 0.1 sec with a spacecraft mass of 1650 slugs. Therefore, the ΔV is

$$\Delta V_{PSA} = \frac{F\Delta t}{m} = 2.182 \times 10^{-3} \text{ ft/sec} \iff \Delta V_{PSA,peraxis} = 1.256 \times 10^{-3} \text{ ft/sec} \tag{29}$$

Given that this will run every 6 minutes,

$$Q_{PSA} = \frac{\sigma^2_{\Delta V,PSA,Per\,Axis}}{360\,\text{sec}} = 4.408 \times 10^{-9} \text{ ft}^2/\text{sec}^3 \tag{30}$$

[†]Email correspondence from John Lewis and Chris Delnero

The Quiescent Process Noise

The combination of these three events is

$$Q_{Quiescent}^{50\,\text{slews}} = Q_{PSA} + Q_{AttSlews}^{50\,\text{slews}} + Q_{AttDeadband} = 3.801 \times 10^{-8}\ \text{ft}^2/\text{sec}^3 \tag{31}$$

This results in

$$Q_{Quiescent}^{50\,\text{slews}} = 3.531 \times 10^{-9}\ \text{m}^2/\text{sec}^3 \tag{32}$$

For the case of a pan/tilt optical camera and 36 slews, the quiescent process noise is

$$Q_{Quiescent}^{36\,\text{slews}} = Q_{PSA} + Q_{AttSlews}^{36\,\text{slews}} + Q_{AttDeadband} = 2.8667 \times 10^{-8}\ \text{ft}^2/\text{sec}^3 \tag{33}$$

This results in

$$Q_{Quiescent}^{36\,\text{slews}} = 2.663 \times 10^{-9}\ \text{m}^2/\text{sec}^3 \tag{34}$$

For the case of a pan/tilt optical camera and 24 slews, the quiescent process noise is

$$Q_{Quiescent}^{24\,\text{slews}} = Q_{PSA} + Q_{AttSlews}^{24\,\text{slews}} + Q_{AttDeadband} = 2.067 \times 10^{-8}\ \text{ft}^2/\text{sec}^3 \tag{35}$$

This results in

$$Q_{Quiescent}^{24\,\text{slews}} = 1.920 \times 10^{-9}\ \text{m}^2/\text{sec}^3 \tag{36}$$

For the case of a pan/tilt optical camera and 12 slews, the quiescent process noise is

$$Q_{Quiescent}^{12\,\text{slews}} = Q_{PSA} + Q_{AttSlews}^{12\,\text{slews}} + Q_{AttDeadband} = 1.266 \times 10^{-8}\ \text{ft}^2/\text{sec}^3 \tag{37}$$

This results in

$$Q_{Quiescent}^{12\,\text{slews}} = 1.176 \times 10^{-9}\ \text{m}^2/\text{sec}^3 \tag{38}$$

The Active Process Noise

Finally, there is the case of the ammonia sublimator, which runs occasionally. The sublimator vents ammonia (NH_3) when the vehicle is close to the moon (due to the increased thermal environment) and after CM/SM separation. When it operates, it imparts a ΔV on the vehicle. It is expected that the sublimators will run for 1/2 hour behind the moon and 1/2 hour before EI. For the CM/SM configuration,

$$\Delta V = \frac{F\Delta t}{m} = \frac{0.8\text{lbf} \times 1800\text{sec}}{1650\text{slugs}} = 0.873\,\text{ft/s} = 0.266\,\text{m/s} \tag{39}$$

For the CM only (entry) configuration,

$$\Delta V = \frac{F\Delta t}{m} = \frac{0.8\text{lbf} \times 1800\text{sec}}{673\text{slugs}} = 2.140\,\text{ft/s} = 0.652\,\text{m/s} \tag{40}$$

This means that

$$Q_{sublime_{CM/SM}} = \left(\frac{0.266}{\sqrt{3}}\right)^2 /1800\,\text{sec} = 1.310 \times 10^{-5}\ \text{m}^2/\text{sec}^3 \tag{41}$$

$$Q_{sublime_{CM\ only}} = \left(\frac{0.652}{\sqrt{3}}\right)^2 /1800\,\text{sec} = 7.877 \times 10^{-5}\ \text{m}^2/\text{sec}^3 \tag{42}$$

It may well be that we will be able to sense the sublimator vents; if this is the case, then the process noise would be reduced, though this would be the case only for the on-board navigation state; the ground-based navigation solution would not be affected.

Summary of Unmodeled Accelerations

Table 1 contains a summary of the previously described unmodeled acceleration as well as their relative strengths.

Table 1. Type and Strength of Unmodeled Acceleration

Type of Noise	Assumptions	Strength (m^2/s^3)
Attitude Deadbanding	Jet firing every 30 minutes	2.313×10^{-11}
Attitude Slewing	50 attitude events	3.098×10^{-9}
Attitude Slewing	25 attitude events	1.601×10^{-9}
PSA Vents	Every 6-10 minutes	4.095×10^{-10}
Ammonia Sublimator	In Lunar Vicinity (0.5 hour)	CM/SM: 1.310×10^{-5}
Ammonia Sublimator	0.5 hour prior to EI	CM Only: 7.877×10^{-5}

RESULTS

The trajectory under consideration a 8 day trajectory departing on December 15, 2017. It is shown in Figure 2.

For this analysis, we included three sets of navigation concepts of operations: 1 hour optical passes, continuous optical passes, and ground tracking only passes. The second case (continuous optical navigation) serves as a bounding case to demonstrate the best performance of the navigation system were we able to get continuous measurements. Currently, it is not clear where and how the optical camera will be mounted. If it is not mounted on a pan/tilt platform, there will need to be attitude maneuvers to obtain optical imagery for navigation. For the first case, we assumed that there would be one hour of optical passes to the closest body; due to thermal and other operational constraints, we will not be able to point the cameras at the nearest body for more than an hour. This is expected to be the most reasonable optical navigation concept of operations for this scenario. In this case, we would commence tracking two hours prior to each maneuver and terminate the pass one hour prior to each maneuver. The concept of operations for ground tracking is as follows: after a period of tracking by ground stations, a navigation state (with associated covariance matrix) will be uplinked to the spacecraft one hour prior to the maneuver. This state would be used to compete and perform the maneuver. This computation of the maneuver could either be done on-board or on the ground.

The optical camera was assumed to have a noise of 5 arc-seconds (1σ) and a bias of 3.33 arc-seconds. In addition the stellar sub-point had a noise of 10 arc-seconds (1σ) and a bias of 5 arc-seconds. Finally the horizon had a noise of 10 km (1σ) and a bias of 3 km.

We assumed that there were 7 Trajectory Correction Maneuvers performed. They were chosen reflective of what was done during Apollo and will likely be adjusted, but they serve as reasonable place-holders, taking into account factors such as crew sleep and time since the previous maneuver. In order to ensure accurate delivery a maneuver was placed 6 hours prior to both Lunar Flyby and Entry Interface (EI). The TCMs are detailed in Table 2.

The TCM performance for the three cases are presented in Table 3.

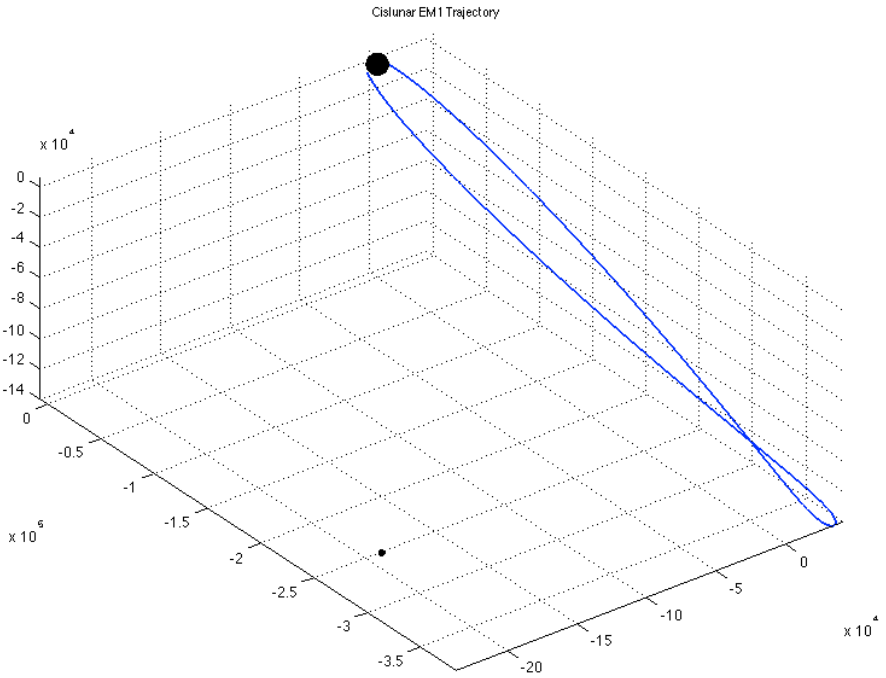

Figure 2. EM-1 Trajectory

Table 2. TCM Locations

TCM 1	TLI + 6 hours
TCM 2	TLI + 1 day
TCM 3	Lunar Flyby - 22 hours
TCM 4	Lunar Flyby - 6 hours
TCM 5	Lunar Flyby + 18 hours
TCM 6	EI - 21 hours
TCM 7	EI - 6 hours

Table 3. 3σ **TCM** ΔV **Performance (m/s)**

	One Hour Optical	Continuous Optical	Ground Tracking
TCM 1 ΔV (m/s)	5.14	5.14	5.16
TCM 2 ΔV (m/s)	0.96	1.02	0.19
TCM 3 ΔV (m/s)	1.55	0.81	0.18
TCM 4 ΔV (m/s)	0.32	0.24	0.31
TCM 5 ΔV (m/s)	1.53	1.45	1.81
TCM 6 ΔV (m/s)	3.52	1.08	0.66
TCM 7 ΔV (m/s)	2.80	0.90	0.71
Total ΔV (m/s)	15.82	10.64	9.03

The Entry Flight Path Angle (FPA) delivery (at Entry Interface) for each of these cases is included in Table 4.

Table 4. 3σ **Delivery Entry Flight Path Angle**

	One Hour Optical	Continuous Optical	Ground Tracking
3 σ Entry Flight Path Angle (deg)	0.252	0.093	0.046

Whereas one can obtain some information regarding navigation and dispersion errors in terms of position and velocity, it is most helpful and illuminating to map these (instantaneous) errors to the entry flight path angle, because that is the quantity of ultimate relevance for being able to successfully complete the mission. This was done by means of state transition matrices, which were used to map the instantaneous navigation and dispersion errors to the time of entry interface and then using the partials of flight-path angle with respect to the state to complete the process.

CONCLUDING COMMENTS

This paper has detailed the navigation error and trajectory dispersion for the EM-1 Free Return mission. It has determined that with one hour of tracking, the navigation performance is sufficient to meet the entry flight angle delivery error of 0.27 degrees (3 σ).

REFERENCES

[1] K. Hill and G. H. Born, "Autonomous Orbit Determination from Lunar Halo Orbits Using Crosslink Range," *Journal of Spacecraft and Rockets*, Vol. 45, May-June 2008, pp. 548–553.

[2] M. L. Psiaki and J. C. Hinks, "Autonomous Lunar Orbit Determination using Star Occultation Measurements," *Guidance Navigation and Control Conference and Exhibit*, Hilton Head, NC, AIAA, 20-23 August 2007.

[3] D. G. Tuckness and S.-Y. Young, "Autonomous Navigation for Lunar Transfer," *Journal of Spacecraft and Rockets*, Vol. 32, March-April 1995, pp. 279–285.

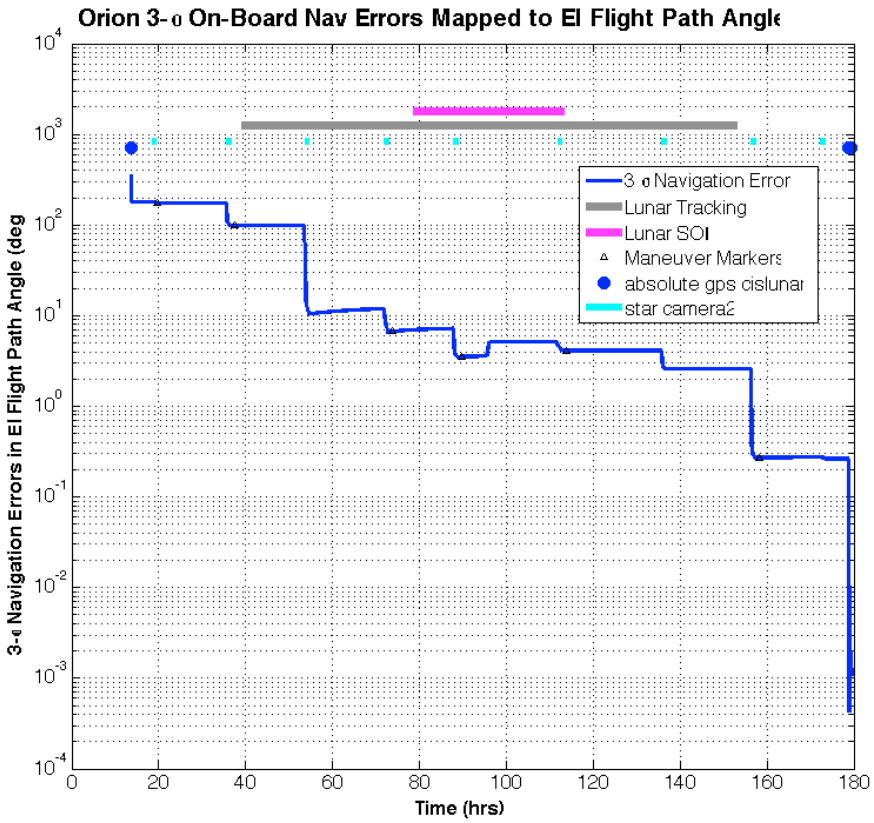

Figure 3. Entry Flight Path Angle Navigation Error (One Hour Tracking)

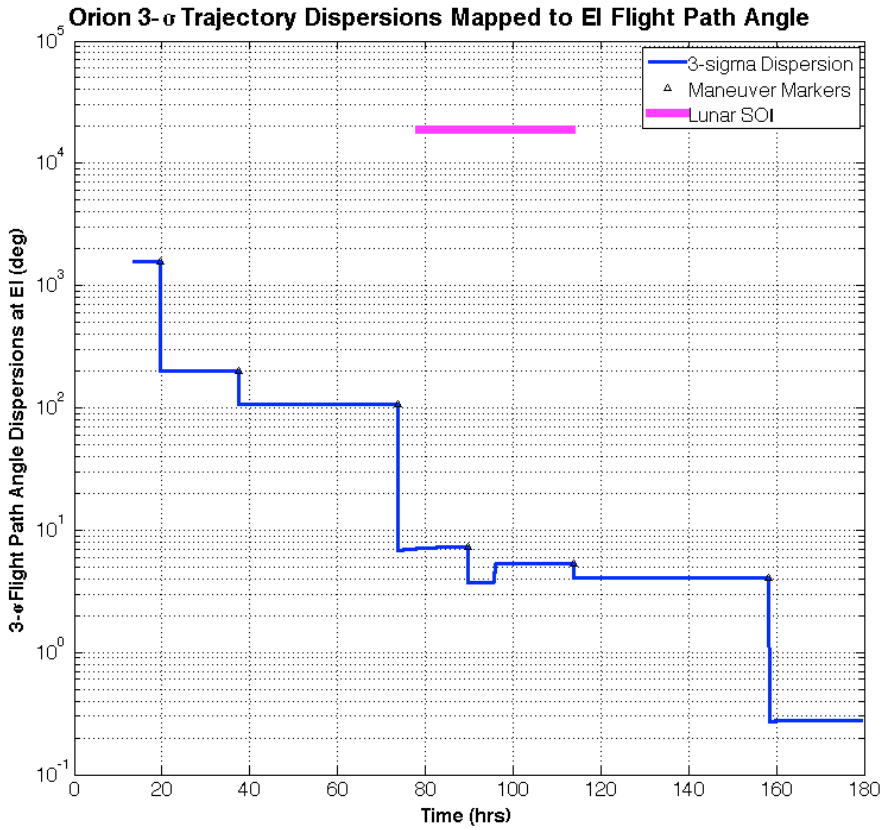

Figure 4. Entry Flight Path Angle Trajectory Dispersion Error (One Hour Tracking)

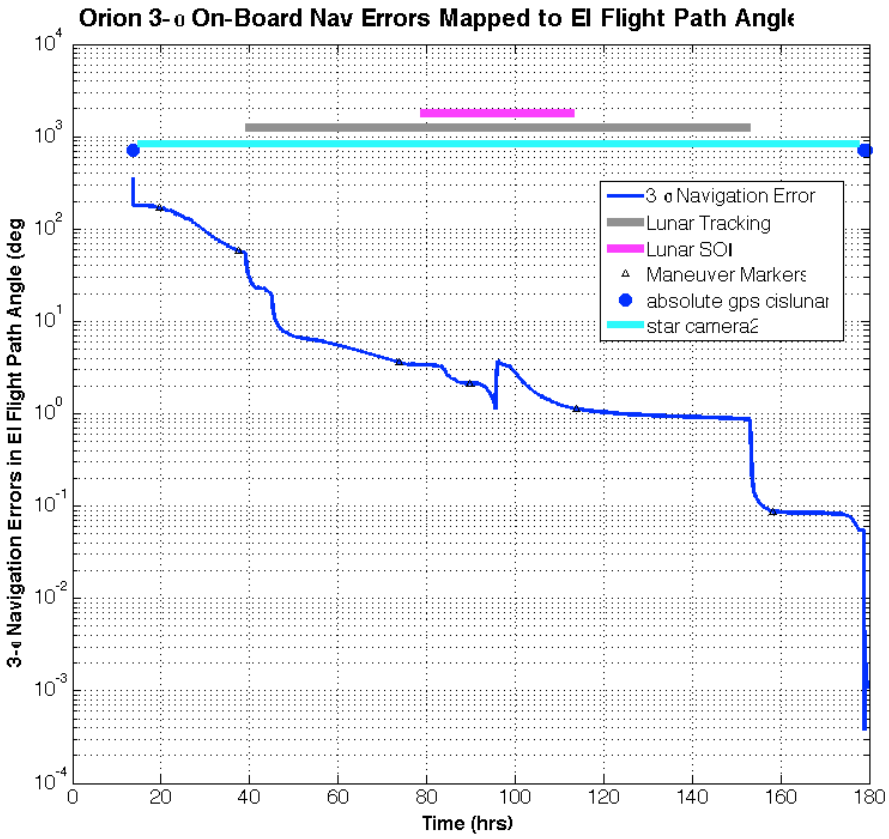

Figure 5. Entry Flight Path Angle Navigation Error (Continuous Optical Tracking)

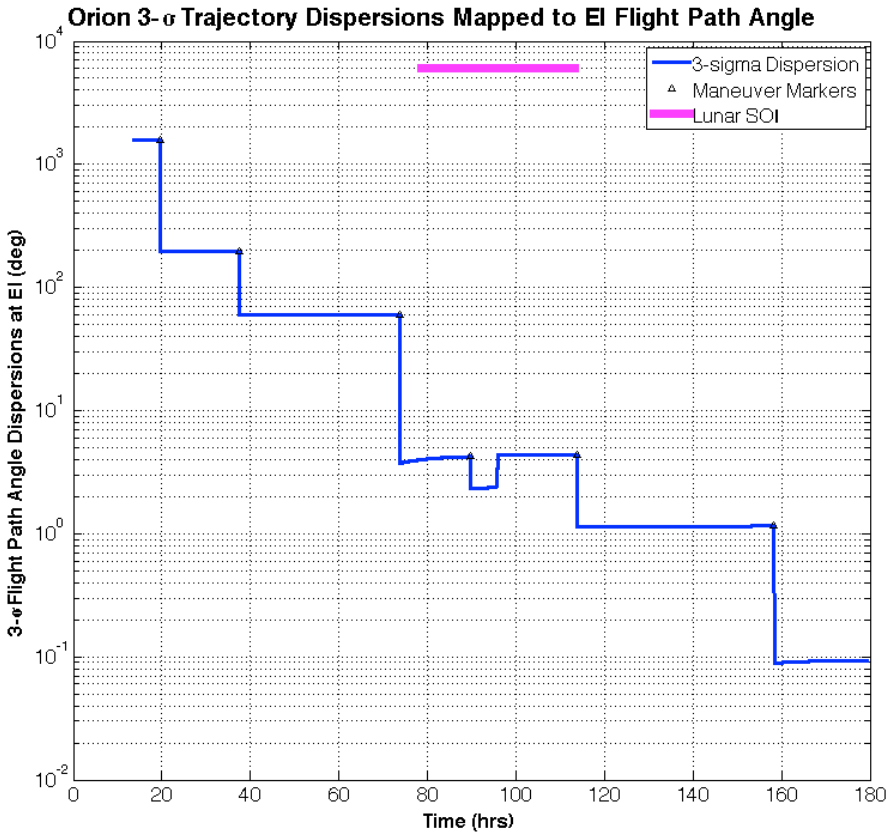

Figure 6. Entry Flight Path Angle Trajectory Dispersion Error (Continuous Optical Tracking)

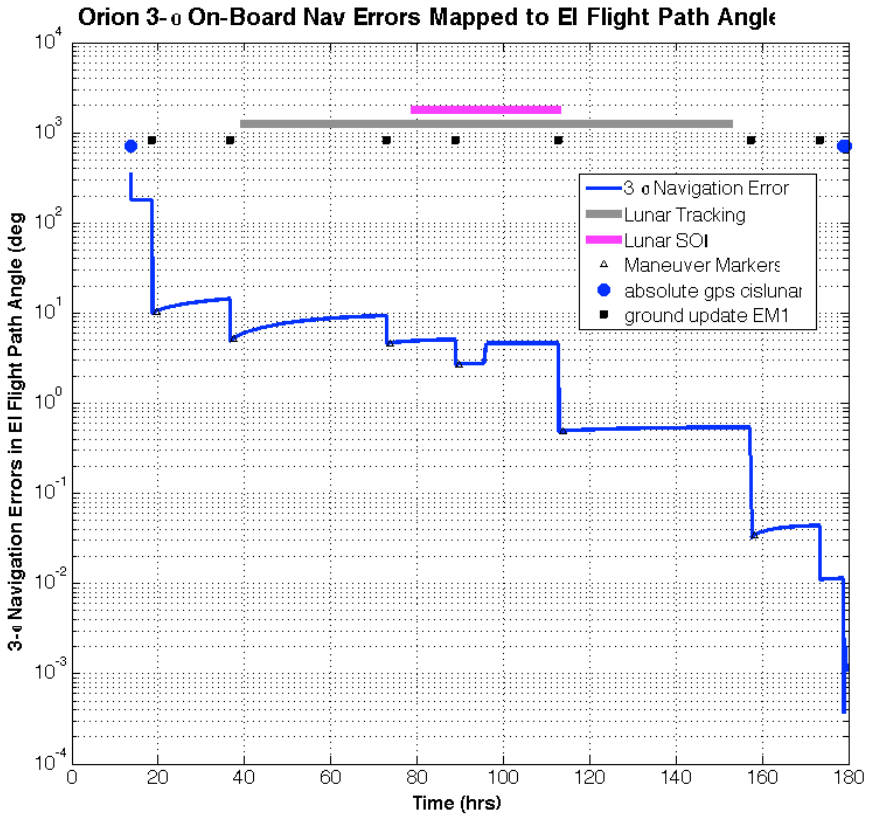

Figure 7. Entry Flight Path Angle Navigation Error (Ground Tracking Only)

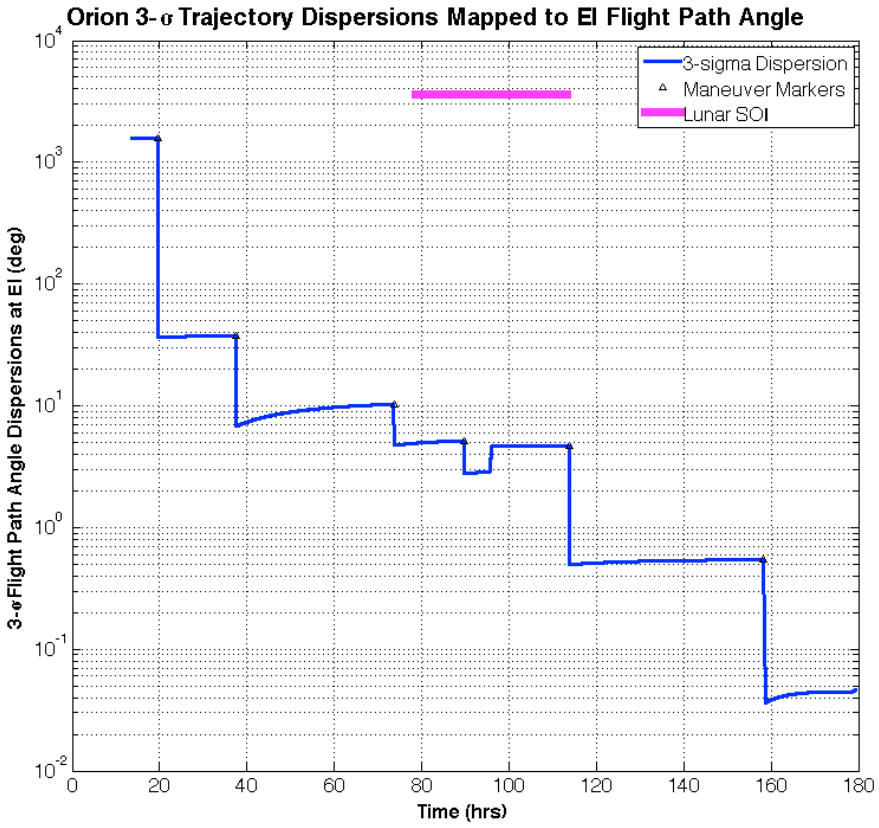

Figure 8. Entry Flight Path Angle Trajectory Dispersion Error (Ground Tracking Only)

[4] R. Zanetti, "Autonomous Midcourse Navigation for Lunar Return," *Journal of Spacecrafts and Rockets*, Vol. 46, No. 4, July–August 2009, pp. 865–873.

[5] J. A. Christian and E. G. Lightsey, "Review of Options for Autonomous Cislunar Navigation," *Journal of Spacecrafts and Rockets*, Vol. 46, No. 5, September?October 2009, pp. 865–873.

[6] P. S. Mayback, *Stochastic Models, Estimation, And Control Volume 1*. Mathematics in Science and Engineering, Orlando, FL: Academic Press, 1979.

[7] D. K. Geller, "Linear Covariance Techniques for Orbital Rendezvous Analysis and Autonomous Onboard Mission Planning," *Journal of Guidance Control and Dynamics*, Vol. 29, November-December 2006, pp. 1404–1414.

[8] R. H. Battin, *An Introduction to the Mathematics and Methods of Astrodynamics*. AIAA Education Series, New York, NY: American Institude of Aeronautics and Astronautics, 1987.